A 3D-SENSOR FOR THE MEASUREMENT OF PARTICLE CONCENTRATION FROM IMAGE SEQUENCES

Peter Geißler [1]   Bernd Jähne [1,2]

[1] Interdisciplinary Center for Scientific Computing   [2] Scripps Institution of Oceanography
University of Heidelberg   Physical Oceanography Research Division
INF 368, D-69120 Heidelberg, FRG   La Jolla, CA 92093-0230, USA
Peter.Geissler@iwr.uni-heidelberg.de   bjaehne@giotto.iwr.uni-heidelberg.de

Commision V, Working Group V/III

KEY WORDS: Camera,Depth-from-Focus,Experiment,Optical,Sensor,Three-dimensional,Underwater

ABSTRACT

A sensor for the measurement of the concentration and size distribution of small particles is described. The particles are visualized by a light blocking technique and imaged by a CCD camera. The concentration measurement is based on a depth-from-focus approach to determine the positions of the particles in three-dimensional world coordinates. From these coordinate sets of all observed particles both the measuring volume as well as the concentration can be determined. The sensor has been developed for the underwater measurement of size distributions of air bubbles submerged by breaking waves to investigate the influence of air entrainment to air-sea gas exchange.

1 INTRODUCTION

The investigation of the exchange of clima-relevate trace gases such as CO_2 and oxygen is a current research topic in modern oceanography. The underlying physical processes are still poorly understood. At low windspeeds, gas exchange is controlled by molecular diffusion through the air/sea phase boundary. With increasing windspeed the situation changes dramatically. Breaking waves entrain air in form of gas bubbles directly to the water. During their lifetime underneath the water surface, these bubbles form an additional reservoir which exchanges its gas contents with the water. Indeed, a strong increase of the gas exchange rates is found when waves start to break [Merlivat,83]. The influence of the air bubbles strongly depends on parameters such as life time, penetration depth and the amount of gas confined. All these parameters are determined by the size of the bubbles. Therefore precise measurements of bubble size spectra and their dependence on wind speed are necessary.

To investigate the properties of air bubble distributions, we have developed an optical sensor which images bubbles on a CCD camera. This allows for a instrument which causes only low flow disturbances. The need to place the measurement volume as far away from the instrument as possible and to image bubbles in a size range of 20 μm to 1000 μm with a suitable resolution causes a narrow depth of field. Therefore, blur in the images is introduced in a natural way, causing only bubbles near the focal plane to be imaged sharply. With increasing distance from the focal plane (subsequently denoted by 'depth') the images of the bubbles become blurred. With our technique this blur is used to determine their depth and, consequently, their three-dimensional position in real world coordinates. From these data, both the measuring volume as well as the size distribution is determined.

This paper will describe the sensor and the image processing techniques used to determine the size distributions from the image sequences. The sensor is also suitable for other types of particles in gases or liquids, provided they are of uniform shape and their refractive index is different from that of the surrounding medium.

2 DEPTH-FROM-FOCUS BASED CONCENTRATION MEASUREMENT

2.1 Introduction to Depth-from-Focus

The processes of imaging a three-dimensional scene onto a two-dimensional sensor at a first glance causes the loss of depth information. Obviously depth recovery needs additional information. For example, stereo imaging can be used to partly reconstruct the distance of objects from two images. Another approach is the use of blur in the images for depth reconstruction. In contrast to a pinhole camera which images every point in object space to an ideal point on the image plane, a lens with finite aperture images only object points on the focal plane to points on the image plane. Increasing distance from this plane then causes an increase of blur in the image (Fig. 1).

Depth-from-focus techniques estimate the grade of blur and correlate it with the distance of the objects from the focal plane. The depth resolution depends on the change of blur with the distance from the focal plane and is therefore related to the depth of field of the optics. Thus, a small depth of field results in a good depth resolution of a depth-from-focus system.
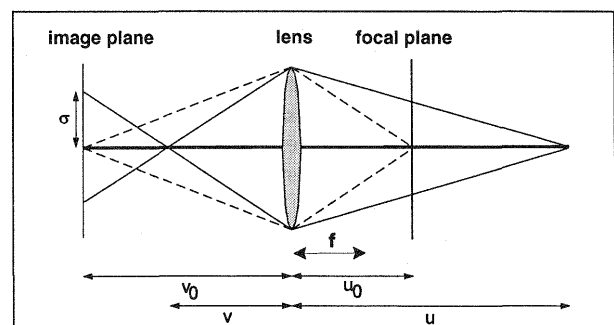

Figure 1: *Defocused imaging: an object point at u_0 is imaged to a point at the conjugated image plane at v_0. A point at $u \neq u_0$ results in a brightness distribution of width σ on the image plane.*

194

International Archives of Photogrammetry and Remote Sensing. Vol. XXXI, Part B5. Vienna 1996

Defocused imaging can be described by the convolution of the well focused image (as it would be with a pinhole lens) with the *point-spread-function* (*PSF*). The PSF is the image of a point object and describes the properties of the optics. Thus

$$\text{spatial domain} \quad G(\vec{x}) = PSF(\vec{x}) \otimes O(\vec{x})$$

$$\updownarrow \qquad\qquad \updownarrow \qquad\quad \updownarrow \qquad (1)$$

$$\text{Fourier domain} \quad \hat{G}(\vec{k}) = \widehat{PSF}(\vec{k}) \cdot \hat{O}(\vec{k})$$

with $O(\vec{x})$ being the object function and $G(\vec{x})$ the resulting image. In Fourier space, defocusing is a multiplication with the Fourier transform of the PSF, the *optical transfer function*. Because multiplication is a commutative operation, it is not possible to distinguish between properties of the object and of the PSF from the gray values in the image. The same amount of blur in the image may arise from steep edges and a wide PSF or from smooth edges and a narrow PSF. But measuring depth from blur requires estimating the width of the PSF from blurring, and thus to avoid inclusion of apparent blur caused by object properties. Many depth-from-focus approaches use additional information provided by several images taken from the same scene to solve this problem. As an example depth series and multi-aperture sequences ([Ens and Lawrence,93], [Pentland,87]) may be mentioned here. Taking several images of the same scene with different parameters of the optics allows to determine the width of the PSF independly of object properties. A very simple setup would consist of a pinhole lens and a second lens with finite aperture. The image given by the pinhole lens does not contain blur caused by a PSF and holds all information about the object properties. With that information, depth can be reconstructed from the second image. For partical purpose, systems with several lenses of different aperture are used.

For the investigation of fast moving objects, this approach results in significant experimental effort and can hardly be used. For such applications depth-from-focus techniques which need only a single image are of great advantage. This is only possible if additional information either about the PSF or the objects is introduced. In this application, like in many other technical applications, the shape of the objects is a priori known. The depth-from-focus technique described here uses the knowledge about the shape of the object to compute an object-global measure of blur from a single image.

2.2 Concentration Measurement

The calculation of size distributions from image sequences of particles requires knowledge of number and size of the observed particles as well as knowledge about the measuring volume. Usually, the measuring volume is determined by means of mechanical delimiters. This gives a fixed and easy to handle volume, but also causes flow disturbances which cannot be neglected. To overcome this problem, we use the following approach:
The basic idea of depth-from-focus based concentration measurements is the use of a virtual measuring volume. The camera looks freely into the medium, so that the volume defined by its depth of field is much smaller than the volume observed. Both particles inside the measuring volume as well as particles located far outside are imaged. The small depth of field then results in defocused imaging for most particles. The 3D-positions of all observed particles are now determined: The position perpendicular to the optical axis is directly given by the gray value center of the image of the particle, multiplied
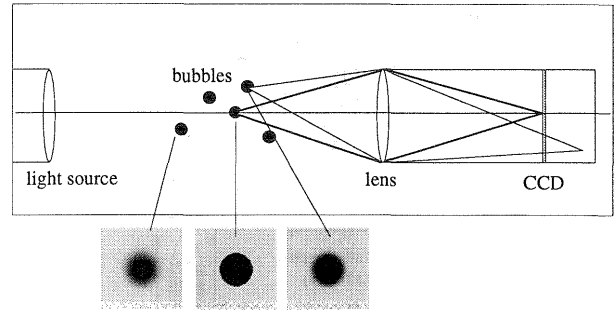

Figure 2: *Principle of depth-from-focus based concentration measurement. The three-dimensional position of each particle is determined from the amount of blur in the image.*

by the magnification of the optics, while the position along the optical axis (subsequently denoted by 'z-coordinate') can be inferred from the defocus (Fig. 2).

If the 3D-positions are known for a suitable long image sequence, the boundaries of the measuring volume can be determined from these data. If a particle is located too far away from the focal plane, the width of the PSF becomes larger than the particle itself. The image is than better described as a 'blurred image of the PSF' than a blurred image of the particle. Therefore no accurate measurement can be done and these particles have to be excluded from the measuring volume. This is done by specifying a minimum value for a measure of the amount of blur. Mechanical delimiters become obsolete to define the measuring volume and are replaced by a *virtual measuring volume* whose boundaries are controlled by the *minimum sharpness criterion*.

To obtain the distribution of particle sizes, in addition to the three-dimensional position the size of each particle has to be measured. The size of blurred particles is not a priori given and has to be defined in a suitable manner. This by some means arbitrary measure of size is then combined with the position to correct for the true size of the particle.

It is important to note that the use of depth-from-focus to measure concentrations requires an adequate visualization method to image the particles in a way suitable for the depth-from-focus technique.

3 THE SENSOR

3.1 Sensor setup

The bubble concentration sensor (*imaging bubble gauge, IBG*) has been used for measurements in the large wind wave tank at Delft Hydraulics (The Netherlands). The device consists of two water tight housings, mounted at the bottom of the flume in a distance of 40 cm (Fig. 3). The measuring volume has a length of several cm in z-direction and is therefore located far away from the device body. The vertical position of the device can be changed, thus allowing the measurement of bubble size distribution at various depths to the mean water surface. One of the housings contains the illumination system, while the optical receiver is located in the other one. The air bubbles are imaged using a CCD camera looking directly into the light source. Light hitting an air bubble in the measuring volume is scattered so that it does not reach the camera lens. Therefore, a dark image of the bubble is obtained on the image plane, allowing the determination of the shape of each individual bubble. Bubbles with a diameter of
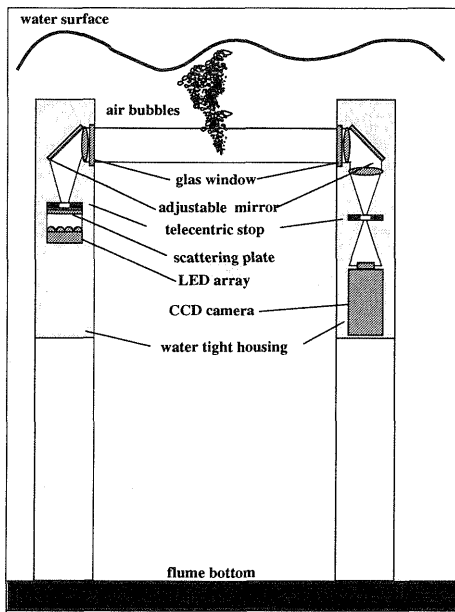
195

International Archives of Photogrammetry and Remote Sensing. Vol. XXXI, Part B5. Vienna 1996

Figure 4: *Two images taken with the IBG device. Both well focused as well as out of focus bubbles can be seen. The bright spot which can be seen in the center of well focused bubbles arises from the small fraction of light (less than 0.1 %) which passes through the bubble.*

Figure 3: *Sketch drawing of the optical bubble measuring device. The left tower contains the illumination optics with the pulsed LED array, the right tower contains the camera together with the imaging optics. The height of the towers can be adjusted from 45 to 100 cm to allow measurements in different distances to the mean water surface.*

less than 1000 μm are of nearly spherical shape and therefore imaged as dark circles (Fig. 4).

The illumination consists of an array of LED's. Synchronized with the image acquisition, they were pulsed with a duration of 20 μs. In addition, the camera is shuttered to an acquisition time of 1/2000 s to completely suppress scattered light from the environment. The short illumination time avoids any motion blur in the images of fast moving bubbles. With a single pixel imaging an area of 10.1 μm × 16.7 μm, bubble velocities up to 0.5 m/s in x-direction and 0.8 m/s in y-direction cause motion blur of less than one pixel. Since typical bubble velocities are less than 30 cm/s and do not exceed 1 m/s motion blur is nearly completely suppressed. Image sequences of 5000 to 8000 images were taken for each measuring condition. They were stored on laser video discs for later processing.

3.2 Position ambiguity

A principal problem of depth-from-focus is that it is not possible to distinguish whether a bubble is located in front or behind the focal plane. The calculation of the true size of a bubble from its blurred size and the amount of blur may therefore result in an ambiguity of the radius measurement. To overcome this problem, we use a telecentric path of rays both on the illumination side as well as on the camera side. With this setup, the aperture stop is located at the rear focal point of the respective optics. The effect is that all principal rays in object space are parallel to the optical axis. Only narrow and axis-parallel ray bundles contribute to image formation. Then, the size of blurred bubbles becomes independent from the grade of the blur or the location along the optical axis. The size of a blurred bubble is hereby defined at the gray values that are the half of the maximum gray value. Furthermore, the grade of blurring becomes independent from whether the position is in front or behind the focal
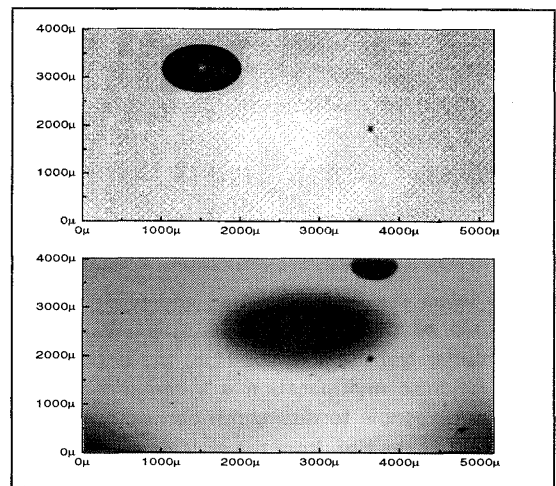
plane. Because of the symmetry introduced by the telecentric path of rays, the position ambivalence can be completely disregarded in the measurements.
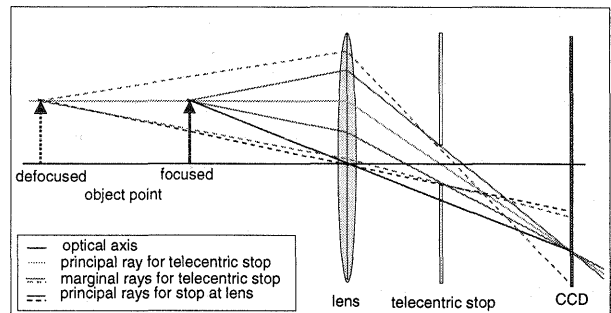

Figure 5: *Comparison of standard and of telecentric path of rays: the displacement of an object point along the optical axis causes changes in the size of the image only with standard optics, but not with telecentric path of rays.*

4 IMAGE PROCESSING TECHNIQUE

The processing of the images to determine the size distribution consists of two main steps: segmentation and depth-from-focus. Before these steps are performed, a brightness normalization is applied to the images to eliminate inhomogeneities and brightness variations of the illumination.

4.1 Brightness normalization

A good understanding of the image formation process and a normalization of the gray values, which is independent of brightness fluctuations and inhomogeneities is an essential requirement for the depth-from-focus technique. The normalization is done by applying a linear illumination model assuming that the measured gray values $g(\vec{x})$ are further proportional to the irradiance $I(\vec{x})$. Then

$$g(\vec{x}) = a(\vec{x})I(\vec{x}) + b(\vec{x}). \tag{2}$$

The unknown quantities $b(\vec{x})$ and $a(\vec{x})$ are obtained by tak-

196

ing a background image $g_b(\vec{x})$ with illumination switched off ($I(\vec{x}) = 0$) and a zero image $g_z(\vec{x})$ in which no bubbles are present ($I(\vec{x}) = I_0(\vec{x})$).

If we describe the objects by their light absorbing coefficient $\tau(\vec{X})$ in the object plane (capitals denote object plane coordinates and small letters denote image plane coordinates) their image is given by :

$$I(\vec{x}) = v(\vec{x}) \left[1 - \tau \left(\frac{\vec{x}}{V_g(z)} \right) * PSF_z(\vec{x}) \right] \qquad (3)$$

with $v(\vec{x})$ describing vignetting and $V_g z$ being the magnification.

Then, the linear inhomogeneous point operation

$$n(\vec{x}) = \frac{g_z(\vec{x}) - g(\vec{x})}{g_z(\vec{x}) - g_b(\vec{x})} = 1 - \frac{I(\vec{x})}{I_0(\vec{x})} = \tau \left(\frac{\vec{x}}{V_g(z)} \right) * PSF_z(\vec{x})$$

$$(4)$$

results in a normalized gray value n in the range of 0 to 1.

4.2 Segmentation

The image processing step of the segmentation distinguishes objects from the background and calculates their apparent (blurred) size. After the depth-from-focus calculation has been performed, the apparent size is corrected to the true particle size. Because blur causes the originally step edges of the objects to become flat, the boundary of a blurred object is not a priori well defined. Therefore we define the boundary to be at these locations where the gray value has decreased to the $1/q$-th of the maximum gray value (Fig. 6). The method used to segment the bubbles is a two-step approach which combines a pre-segmentation step with a fast region growing algorithm. Bubbles within the largest possible size of the measuring volume show a plateau with a gray value of 1 in the normalized image. At the very border of that volume, the plateau shrinks to a single point. Beyond this maximum distance from the focal plane, the width of the PSF exceeds the size of the (well-focused) image of the bubble. For that reason it is no longer possible to calculate size and depth from the blurred image and therefore it is not necessary for the pre-segmentation to detect those bubbles. Because all bubbles which may be within the measuring volume have to show a
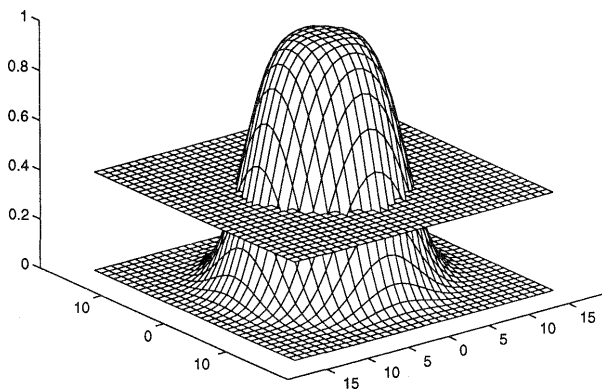
maximum gray value of about 1 and the background has been made uniform by the normalization, pre-segmentation can be carried out by a global thresholding. It is important to note that the value of the threshold does not affect the result of the segmentation, since it is guaranteed that all bubbles within the measuring volume are found as long as the threshold is within a sensible range, e.g. 0.2 to 0.8.

The exact boundary of a bubble is found by the second step, the region-growing algorithm. This algorithm is a modification of a region growing method developed by [Hering et. al,95] and shall be briefly described here. The initial step of a region growing segmentation is the detection of *seeding points* as starting locations for the growing. With our algorithm, seeding points are defined as the location of the gray value maximum of each object. The image is smoothed by a small binomial filter to reduce noise and therefore avoid mislocating the maximum due to random noise peaks. The region growing phase starts with each seed defining different objects, which consists of this single pixel each. Pixels are than added to the objects if their gray value is larger as $1/q$ times the gray value of the initial seeding point and if they are 8-neighbors of the current boundary line of the object. The growing phase stops if no new object pixels can be found. The region growing procedure causes the objects to be connected and to have the correct size regardless of their size in the starting image provided by the thresholding. Fig. 7 shows the final result of the segmentation for several bubbles.
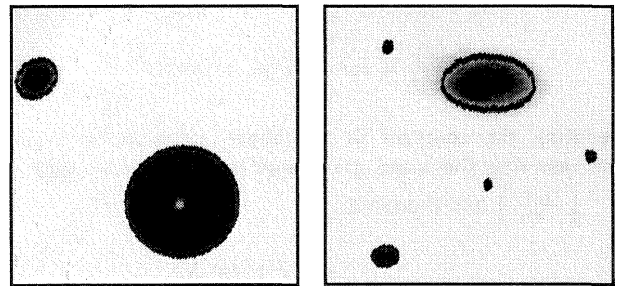

Figure 7: *Final segmentation result of two images. The gray lines indicate the boundary of the particles (obtained with $1/q = 1/e$).*

4.3 Depth-from-Focus

A usual approach for depth-from-focus is to calculate a measure of blur at each image point. Thus a depth-map of the image can be calculated which contains the distance from focal plane for each pixel. This is only possible if more than one image of the same scene is available, due to the impossibility to distinguish between PSF and object function from the gray value image. A modification of this approach for one-image depth-from-focus has been given by [Lai et al.,92] who uses the assumption of a Gaussian shaped PSF. At step edges the standard deviation of the Gaussian is estimated and at these points a depth map is calculated. Different from calculating a depth-map, our approach performs the object detection first and then does an object-oriented depth-from-focus, measuring the amount of blur of complete objects. This allows for a fast depth determination, suitable for the evaluation of long image sequences.

A good integral measure of the blur of a particle is the mean gray value g_m on the segmented area. With increasing blurring, the edges of the particles become less steep and therefore the mean gray value decreases (Fig. 8 and 11).
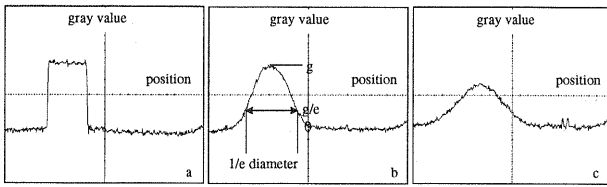

Figure 6: *Definition of the $1/q$-area as the size of blurred objects. As an example, the image shows a blurred object and it's boundary given by the intersection with the $1/q = 0.4$ plane.*

197

International Archives of Photogrammetry and Remote Sensing. Vol. XXXI, Part B5. Vienna 1996

Figure 8: *Radial cross section through the gray value distribution of bubbles at different distance from the focal plane. The distance increases from left to right.*

The fact that the shape of the point-spread-function is independent of the distance z allows the PSF to be expressed in terms of a general shape function $B(\vec{x})$ and a scaling factor $V_p(z)$:

$$PSF_z(\vec{x}) = kB\left(\frac{1}{V_p(z)}\vec{x}\right) \qquad (5)$$

with the normalization factor $k^{-1} = \int d\vec{x}B(\vec{x})$. At the focal plane $(z = 0)$ V_p is zero, resulting in a delta function for the PSF. This can be used to analyze the behavior of g_m in more detail:

All bubbles with the same ratio between the radius r' and the size V_p of the point spread function have the same mean gray value g_m, because their images differ only in size and are of the same shape. Thereby $r' = V_g(z)r$ is the radius of the well focus object of radius r on the image plane. Thus

$$\frac{V_p(z)}{V_g(z)r} = const \Leftrightarrow g_m = const. \qquad (6)$$

Denoting the constant in the above equation by $\gamma(g_m)$ and resolving the mean gray value is given by $g_m(z,r) = \gamma^{-1}\left(\frac{V_p(z)}{r}\right)$ and therefore

$$g_m(z,r) = g_m\left(\frac{V_p(z)}{V_g(z)r}\right) \qquad (7)$$

If we use a telecentric path of rays the magnification V_g becomes independ from z and with the use of $q = 1/2$ for segmentation the $1/q$-area represents the true size of the particles. Furthermore, $V_p(z)$ is then a symmetric and linear function of z. Therefore, g_m depends only on the normalized distance z/r:

$$g_m(z,r) = \gamma^{-1}\left(\frac{a|z|}{r}\right) = g_m\left(\frac{|z|}{r}\right) \qquad (8)$$

5 CALIBRATION

Calculating bubble size distributions from the image sequences with the depth from focus approach requires that the instrument is carefully calibrated with a focus series of calibration targets of known size. Patterson reticles were used as calibration targets. This standard target for microscopic calibration consists of a series of black circles in a diameter range from 18 μm up to 450 μm on a glass plate (Fig. 9). Because Patterson globes are not absolutely accurate, the true size of each circle has to be measured independently, e.g. using a calibrated microscope. A black circle is a very good approximation of the focused image of a bubble, since with the optical setup used in the experiments more than 99.6 % of

the incident light is scattered away from the receiver. Nevertheless, the bright dot which appears in the center of well focused bubbles can be easily removed by applying a median filter to the normalized image. Depth series centered at the
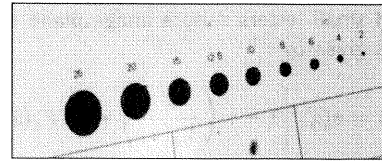

Figure 9: *Partial view of the calibration target.*

focal plane are taken with a step size of 1 mm. Fig. 10 shows the radii measured from different circles of the Patterson target. Within the measuring volume, the difference between the measured and the true radius in in the order of 10 to 15 μm, which is about the size of one pixel. The variation of the mean gray value with increasing depth is shown in Fig. 11. A linear model $g(z,r) = g_0 - \alpha(r)|z|$ fits well to the data. Because a small axis offset and slight tilt of the target can often not be avoided, the axis offset for each circle is corrected by finding the center of symmetry in its depth series.
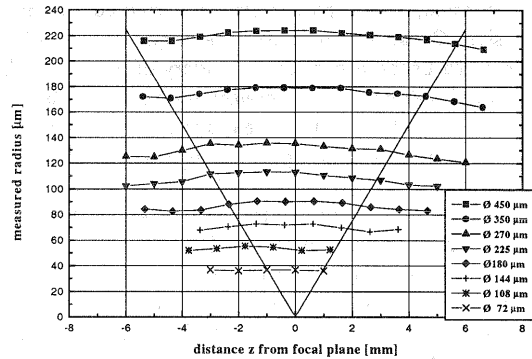

Figure 10: *Independence of the size of blurred bubbles with the distance from the focal plane. The thin lines indicate the maximum size of the virtual measuring volume.*

6 CALCULATION OF PARTICLE CONCENTRATION

6.1 Determination of the measuring volume

The decrease of the mean gray value with increasing distance from the focal plane can now be used to define the measuring volume by a lower limit for g_m. Only bubbles with mean gray values above this limit are taken into account for the calculation of the size distribution. Thus the linear dependence of g_m on the normalized distance

$$g(z,r) = g_0 - \alpha(r)|z| = g_0 - \alpha_0\frac{|z|}{r} \qquad (9)$$

gives the volume boundary:

$$z_{max} = \frac{1}{\alpha(r)}(g_0 - g_{min}) = \frac{r}{\alpha_0}(g_0 - g_{min}). \qquad (10)$$

The measuring volume is then given by

$$V(r) = 2z_{max}(r)A_0 \qquad (11)$$

with A_0 being the area imaged by the CCD at the focal plane. The depth of the volume is controlled by the parameter g_{min}.
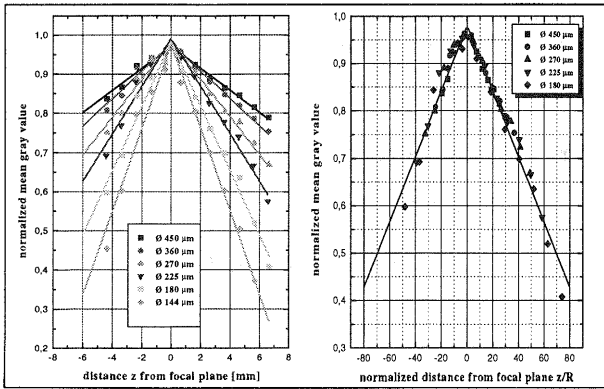
198

Figure 11: *left: mean gray value calculated for different Patterson globes; right: mean gray value versus normalized distance z/R. This validates the fact that g_m only depends on z/R.*

It is important to note that the volume depends on particle size and increases with larger particles, because a large particle becomes less blurred compared to a smaller particle if its image is convolved with the same PSF.

6.2 Calculation of true particle size

As mentioned above with a telecentric path of rays the true particle size can be easily obtained from the segmentation of the images. Due to the symmetry between particles located at the same distance, but in front or behind the focal plane, the intrinsic ambivalence does not cause an ambivalence in the depth or size measurement and can be ignored completely. The situation is different with standard optics where the aperture stop is not located at the back focal plane of the lens system. Then V_g depends on z and the segmented size does not necessarily meet the true size. The fact that there is a unique relation for the true radius r and the depth z of an object to the two measurable parameters, g_m and the segmented radius r_q can be used to solve the problem [Geißler and Jähne,95a]. The relation between the four parameters are obtained from the calibration depth series. The values of the output parameters (r, z) are mapped on a regular grid in the input parameter set (r_q, g_m) and used as a fast look-up table to perform the calculation.

6.3 Size distributions

Segmentation and depth-from-focus result in the knowledge of position and size of the particles observed in an image. The data from a suitable long image sequence is needed to calculate size distributions. The result of the segmentation of an image sequence is shown in Fig. 12. Due to the fast segmentation and depth-from-focus, evaluation of an image
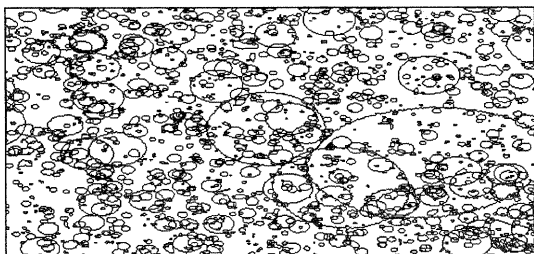

Figure 12: *Result of the segmentation of an image sequence. The dark gray lines indicate the boundary lines of the bubbles.*
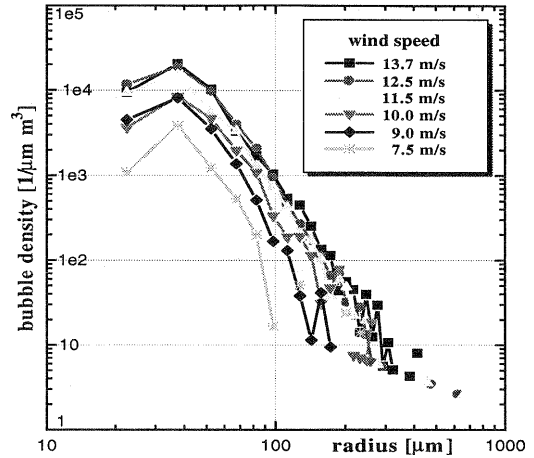

Figure 13: *Fresh water bubble size spectra measured at different wind speeds in the large wind/wave flume of Delft Hydraulics.*

can be done in less than one second on a 40 MHz i860 RISC processor system.

Bubble size distributions were calculated from the number $N(r, dr)$ of bubbles found in the radius interval $[r, r + dr]$ by

$$\psi(r, dr) = \frac{N(r, dr)}{N_I \, dr \, V(r)} \qquad (12)$$

where N_I is the total number of images. As an example, Fig. 13 shows some fresh water bubble size distributions measured in the large wind/wave flume of Delft Hydraulics. These measurements have been described in greater detail in [Geißler and Jähne,95b].

REFERENCES

[Ens and Lawrence,93] Ens, J., Lawrence, P.: 1993, 'An investigation of methods for determining depth-from-focus', *IEEE Trans. PAMI, 15, 97–108*

[Lai et al.,92] Lai, S. H., Fu , C. W., Chang, S. Y.: 1992, 'A generalized Depth Estimation Algorithm', *IEEE Trans. PAMI, 14, 405–411*

[Merlivat,83] Merlivat, L., Memery, L. , 'Gas Exchange Across an Air-Water Interface: Experimental Results and Modeling of Bubble Contribution to Transfer', *Jour. of Geophysical Res.* Vol.88, pp.707 - 724, 1983

[Geißler and Jähne,95a] Geißler, P., Jähne, B.: 'One-Image Depth from Focus for Concentration Measurements', *Proc. of ISPRS Intercommission Workshop 'From Pixels to Sequences', Zurich, March 22 - 24.* In Int'l Arch. of Photog. and Rem. Sens., Vol 30, Part 5W1, 1995

[Geißler and Jähne,95b] Geißler, P., Jähne, P.: 'Measurements of bubble distributions with an optical technique based on depth from focus', *Air-Water Gas Transfer - Selected Papers from the Third International Symposium of Air-Water Gas Transfer, Heidelberg, ed. by B. Jähne and E. Monahan,* Aeon Hanau, ISBN 3-9804429-0-X, 1995

[Hering et. al,95] Hering, F., Wierzimok, D., Jähne, B.: 'Particle Tracking in Space Time Sequences', *Proc. of the 6th Int'l Conference on Computer Analysis of Images and Patterns, Prague, 294 – 301* in Lecture Notes in Computer Sciences 970, Springer, 1995

[Pentland,87] Pentland, A. P.: 'A new sense for depth of field', *IEEE Trans. PAMI, 9, 523–531*

199

International Archives of Photogrammetry and Remote Sensing. Vol. XXXI, Part B5. Vienna 1996